Calibration and experiment of the contact parameters for the discrete meta-simulation of peanut pods during harvest in saline soils

Zengcun Chang[1], Jialin Hou[1], Baiqiang Zuo[2], Shiyang Yin[3], Dongjie Li[1], Yuanhao Wang[4], Pengcheng Ji[4], Dongwei Wang[2*]

(1. *College of Mechanical and Electrical Engineering, Shandong Agricultural University, Tai'an 271018, China*;
2. *Yellow River Delta Intelligent Agricultural Machinery Equipment Industry Academy, Dongying 257300, China*;
3. *Qingdao Agricultural Technology Extension Center, Qingdao 266071, China*;
4. *College of Mechanical and Electrical Engineering, Qingdao Agricultural University, Qingdao 266109, China*)

Abstract: In this study, a simulation model of peanut pod particles during harvest in saline soil was tested to calibrate contact parameters. Discrete meta-fill models of peanut pods were generated by a 3D meter and EDEM software. The range of values of contact parameters for peanut pods was measured by conducting collision and other tests using a homemade test rig. The parameters that affect the significance of the simulation process of stacking angle were screened by the Plackett-Burman experiment, the steepest ascent experiment, and the Box-Behnken experiment. An optimization test determined the optimal simulation model parameters: The peanut pods had a Poisson's ratio of 0.386 and a shear modulus of 3.04 MPa. The coefficient of recovery for pods-pods collisions was 0.335, the coefficient of static friction was 0.854, and the coefficient of rolling friction was 0.346. The coefficient of recovery of collision between the pods-65Mn steel was 0.339, the coefficient of static friction was 0.589, and the coefficient of rolling friction was 0.159. The test results showed a relative error of 0.42% between the stacking angle bench and simulation tests. The results can provide data support for studying the discrete metamaterial characterization of peanut pods.

Keywords: peanut pods, saline soil, discrete element, contact parameter, stacking angle, calibration and experiment
DOI: 10.25165/j.ijabe.20251804.9692

Citation: Chang Z C, Hou J L, Zuo B Q, Yin S Y, Li D J, Wang Y H, et al. Calibration and experiment of the contact parameters for the discrete meta-simulation of peanut pods during harvest in saline soils. Int J Agric & Biol Eng, 2025; 18(4): 53–62.

1 Introduction

Peanut is an important oil and cash crop in China. Peanuts are loved for their high nutritional value due to their rich fat and protein content. In China, peanuts are grown in a wide range of regions and areas[1,2]. China's peanut planting area accounts for about 17.5% of the world's total[3]. In recent years, with the continuous development of agricultural machinery, the degree of mechanization of peanut harvesting has increased. The variety of peanut harvesting machinery is also increasing. During the peanut digging and harvesting process, it is found that there are complex forces between peanut pods and pods, pods and soil, and soil and digging device. These complex forces easily cause peanut pod damage and poor digging and harvesting results. Complex forces cannot be directly determined by physical tests. Moreover, traditional tests are time-consuming and require many validation proofs, which increases the difficulty of interaction force determination[4]. The unique sticky and heavy nature of saline soils exacerbates the difficulty of digging and harvesting[5]. With the gradual and wide application of the discrete element method in agricultural production, discrete meta-simulation tests can provide a new idea and method for researching low-damage and high-quality peanut harvesting.

In recent years, the discrete element method (DEM) has developed rapidly in agricultural engineering as an important tool for studying the properties of particulate materials. The DEM plays an important role in the experimental study of contact characterization and simulation of agricultural materials[6–10]. Currently, discrete meta-simulation parameter calibration is mainly applied to agricultural materials such as soil, seed, and fertilizer. Sun et al. used the Hertz-Mindlin with JKR Cohesion contact model in EDEM to calibrate the simulation parameters of typical sloping clay soil[11]. Relevant simulation contact parameters were obtained for typical clayey soils on slopes. Song et al. used experimental and simulation methods to simulate the calibration of soil contact parameters in mulberry orchards[12]. The results lay the foundation for the study of discrete elemental simulation and analysis of the interaction between soil-touching components and soil of mulberry farming machinery. Horabik et al. determined the coefficients of recovery for discrete metamodels of soybean and rapeseed seeds at different water contents by calibrating the simulation parameters[13]. Zhang et al.[14] applied the Hertz-Mindlin with bonding model to

Received date: 2025-01-15 **Accepted date:** 2025-06-04
Biographies: Zengcun Chang, PhD, research interest: economic crop machinery and intelligent equipment, Email: 2021010107@sdau.edu.cn; **Jialin Hou**, PhD, Professor, research interest: Design and theory of agricultural equipment, Email: jlhou@sdau.edu.cn; **Baiqiang Zuo**, Engineer, research interest: agricultural mechanization, Email: zbqqau@163.com; **Shiyang Yin**, Engineer, research interest: agricultural mechanization, Email: ysy264300@163.com; **Dongjie Li**, PhD, research interest: economic crop machinery and intelligent equipment, Email: 2023010064@sdau.edu.cn; **Yuanhao Wang**, MS candidate, research interest: agricultural mechanization, Email: 20232111056@stu.qau.edu.cn; **Pengcheng Ji**, MS candidate, research interest: agricultural mechanization, Email: 20232211008@stu.qau.edu.cn.
***Corresponding author: Dongwei Wang**, PhD, Professor, research interest: design and theory of agricultural equipment. Yellow River Delta Intelligent Agricultural Machinery Equipment Industry Academy, Dongying 257300, China; Tel: +86-13573255789, Email: w88030661@163.com.

construct a model for water chestnuts and carried out the discrete element parameter calibration. Zhang et al.[15] calibrated the simulation parameters of American ginseng seeds by combining physical and simulation tests. The study determined the contact parameters between each part, which provided a theoretical basis for designing and optimizing the sowing machinery of American ginseng. Jia et al.[16] investigated and analyzed the interactions between straw and mechanical components using the discrete element method. The research results provide a scientific basis for post-harvest processing in rice fields. Xu et al.[17] calibrated the flax capsule's discrete element model parameters and optimized the threshing device's operating parameters using EDEM software. Currently, some scholars have constructed fine geometric models of pods of soybean and oilseed rape through CT scanning, laser scanning, and 3D reconstruction techniques. Crop contact parameters were calibrated by combining high-speed camera and force sensor data, among others. However, due to the uneven surface and internal multi-chamber structure of peanut pods, the existing DEM models can only be simplified to ellipsoids or composite spheres. There is almost a gap in the study of podzol-soil bonding and friction coefficient calibration in saline soils. The mechanical coupling with roots and soil during peanut pod growth has not yet been represented in the DEM.

Numerous current studies on parameter calibration of agricultural materials exist. However, fewer studies are available on parameter calibration for peanut pods. In particular, no parameter calibration study of peanut pods in saline clay-heavy soils exists. Saline soils have special physical and chemical properties compared with ordinary soils, and often show the compound stress of "high PH value + high salt + high viscous particles". PH value, salt content, and sticky grain content have important effects on discrete meta-simulation of peanut pods. High salinity, high pH, and high clay particle content all tend to cause changes in the surface charge properties of soil particles, which enhance inter-particle bonding and increases soil hardness and agglomeration effects. Parameters such as critical fracture energy, bond radius, particle size distribution, and elastic modulus of the bonded model in the DEM were changed accordingly. Key parameters such as bond model, particle gradation, and moisture-dependent friction coefficient need to be coupled in the DEM analysis. The parameters such as shear strength and modulus of elasticity of saline soil were determined by triaxial test, and the size distribution of soil aggregates was quantified and the DEM model was calibrated by combining with CT scanning or micro-imaging technology. This study uses the discrete element method to calibrate the contact parameters between peanut pods and machine contact materials through a combination of bench tests and simulation tests to accurately determine the contact parameters of peanut pods during the harvesting period in saline soil. The research results are expected to provide a parametric basis for further research on low-damage digging and harvesting technology for peanuts in saline soil.

2 Experiment materials and methods

2.1 Experiment material

The peanut pod experiment materials were obtained from the Saline Agricultural Experimental Demonstration Base of Dongying Agricultural Hi-Tech Industrial Demonstration Zone, Dongying City, Shandong Province, China. The experiment material was sampled on September 13, 2024. The sampling site is in the temperate monsoon climate zone (37°18′N, 118°39′E, about 6 m above sea level). The peanut variety is Yuhua 18, a salinity-tolerant high-oleic peanut. At the time of sampling, the water content of peanut pods was 36.72%. A sampling of peanut pods was carried out using the "S-shaped" method according to the principles of "randomization, equivalence, and multipoint"[18]. Ten peanut plants were selected to remove all the pods. The pods were counted according to their size and shape, and the number and percentage of pods of different shapes and sizes were statistically determined.

2.2 Discrete meta-filling model construction for peanut pods

2.2.1 Peanut pod 3D model creation

In this study, the Yuhua 18 peanut, the most widely planted peanut in the coastal saline area, was selected to calibrate pod parameters. Yuhua 18 peanut pods are of normal type with medium and light reticulation. The weight of one hundred pods is 227.7 g. The height of the main stem of this variety of peanut plant is 45.3 cm, and the length of the lateral branches is 54.1 cm. The soil salinity is 3%. After statistical and comparative analysis, it was found that peanut pods at harvest time had the following main shapes, as shown in Figure 1. Statistical and comparative analyses show that there are three main types of peanut shapes at harvest time: normal, cocoon, and single-grain ellipsoidal.

a. Normal type b. Normal type c. Single-grain ellipsoidal

Figure 1 Typical different shapes of peanut pods at harvest time

Due to the large differences in the shape of individual peanut pods and the complex mesh structure on their surface, it is impossible to directly model peanut pods in three dimensions. 3D scanning is adopted to construct the geometric model in order to simplify the model and reduce the error between the model and the real object. The outer surface coordinates of the peanut pods were captured, and redundant data points were removed by a fully automated three-dimensional scanning detector (Model: OPSCAN500D; single-side scanning accuracy: 0.005 mm; overall scanning accuracy: ≤0.015 mm) from Zhongce Testing Technology (Hangzhou) Co. Imageware software and the NURBS model were utilized for image smoothing and surface reconstruction[19,20]. The obtained geometric model of peanut pods is shown in Figure 2.

a. Normal type b. Normal type c. Single-grain ellipsoidal

Figure 2 Geometric modeling of peanut pods of different shapes

2.2.2 Peanut pods discrete metamodel filling

Three types of peanut pod geometry models were exported to STL format files. The models were imported into EDEM software and populated using the software's Generate Particle function. Separate attempts were made to use different smoothing degrees during the model-filling process. The smoothness of the filled peanut pod model was analyzed comparatively to find the filled model closest to the real shape. This model was used as a discrete meta-filling model for three types of peanut pods. The populated discrete metamodel of the peanut pods is shown in Figure 3.

2.3 Selection of contact model

The EDEM software was utilized to conduct a simulation contact parameter calibration study, which mainly includes contact

a. Normal type b. Normal type c. Single-grain ellipsoidal

Figure 3 Discrete meta-filling models of peanut pods of different shapes

and collision between peanut pods-pods and pods-steel. The modeling of the contact between the studied objects is the basis of the simulation analysis. Currently, the commonly used contact models in EDEM software are the Hertz-Mindlin (no slip) model, the Hertz-Mindlin with Bonding model, and the Hertz-Mindlin with JKR model.

There is no sticking between peanut pod particles due to their internal or external forces and no heat transfer or abrasion problems. Therefore, the Hertz-Mindlin (no slip) model can be chosen to simulate the interaction between peanut pod particles, pod particles, and mechanical parts[21]. The Hertz-Mindlin (no slip) model is based on Mindlin's research results and usually consists of a combination of an inter-particle normal force model and a tangential force model. The particles are generally assumed to be spherical in discrete element analysis. Assuming that the radii of the two particles where contact occurs are R_1 and R_2, the normal overlap is α. It follows that:

$$\alpha = R_1 + R_2 - |\boldsymbol{r_1} - \boldsymbol{r_2}| \tag{1}$$

where, $\boldsymbol{r_1}$ and $\boldsymbol{r_2}$ are the two particle center position vectors.

The particle equivalent ionic radius R^* can be obtained from Equation (2):

$$R* = \frac{R_1 R_2}{R_1 + R_2} \tag{2}$$

Therefore, the normal force F_n, normal damping force F_n^d, and normal stiffness S_n between particles can be obtained from Equations (3) and (4):

$$F_n = \frac{4}{3} E* \sqrt{R*} \alpha^{\frac{3}{2}} \tag{3}$$

$$\begin{cases} F_n^d = -2\sqrt{\dfrac{5}{6}}\beta\sqrt{S_n m*}\, v_n^{rel} \\ S_n = 2E* \sqrt{R*\alpha} \\ \beta = \dfrac{\ln e}{\sqrt{\ln^2 e + \pi^2}} \end{cases} \tag{4}$$

where, E^* is the equivalent modulus of elasticity, MPa; R^* is the equivalent ionic radius of the particles, mm; α is the normal overlap, mm; m^* is the equivalent mass, kg; v_n^{rel} is the value of the normal component of the relative velocity, m/s; e is the coefficient of recovery; β is the parameter related to the coefficient of recovery.

The inter-particle tangential force F_t and tangential stiffness S_t can be obtained from the following equation:

$$\begin{cases} F_t = -S_t \delta \\ S_t = 8G* \sqrt{R*\delta} \end{cases} \tag{5}$$

where, δ is the tangential overlap; G^* is the equivalent shear modulus.

Then the tangential damping force F_t^d between particles is:

$$F_t^d = -2\sqrt{\frac{5}{6}}\beta\sqrt{S_t m*}\, v_t^{rel} \tag{6}$$

where, v_t^{rel} is the tangential relative velocity.

Rolling friction is a very important and non-negligible factor when simulating with EDEM software. Rolling friction can be considered by adding moments to the particle contact surfaces.

$$T_i = -\mu_r F_n R_i \omega_i \tag{7}$$

where, μ_r is the rolling friction coefficient; R_i is the distance from the center of mass of the particle to the contact point of the two particles, mm; $\boldsymbol{\omega}_i$ is the unit angular velocity vector at the contact point of the two particles, rad/s.

2.4 Selection of contact materials

The mechanical parts of the peanut digging and harvesting process are usually manufactured using 65Mn steel. Therefore, 65Mn steel was selected as the test contact material in this study. Table 1 shows the basic characteristic parameters of 65Mn steel[22].

Table 1 Basic characteristic parameters of the contact material 65Mn steel

Materials	Densities/kg\cdot m^{-3}	Poisson's ratio	Shear modulus/Pa
65Mn steel	7.865×10^3	0.3	7.90×10^{10}

2.5 Determination of basic physical parameters of peanut pods

2.5.1 The process of density determination

Since peanut pod shells are insoluble in water and less dense than water, the drainage method does not allow for direct measurement of the density of peanut pods. Therefore, during the density measurement, the experiment used a rigid plastic rod to press the peanut pods into the water (the rigid plastic rod is tangent to the water's surface). The specific experiment procedure is as follows:

Ten peanut pods were randomly selected from each of the three types of peanut pods counted. The mass of each peanut pod was weighed, and the weighing data were recorded using a high-precision analytical balance (model: YP10002B; precision: 0.01 g) produced by Shanghai Analytical Niu Leibel Instrument Co. Add 50 mL of water to a measuring cylinder with a capacity of 100 mL (accuracy: 1 mL). Place the selected peanut pods into separate measuring cylinders. Press the peanut pods completely into the water using a rigid plastic rod. Record the volume change as the water rises in the measuring cylinder.

2.5.2 The process of determining Poisson's ratio

Poisson's ratio is the absolute value of the ratio of the transverse positive strain to the axial positive strain of a peanut pod when subjected to unidirectional tension or compression. Poisson's ratio is an elastic constant reflecting the lateral deformation of peanut pods. The peanut pods are assumed to be oriented in the axial direction x for length and in the transverse direction y for width. The compression test of peanut pods was carried out using a CMT4503 electronic universal material testing machine at a speed of 10 mm/min. The compression loading time is set to 3 s. The deformation of peanut pods in the length and width directions was measured. The Poisson's ratio of peanut pods was calculated from Equation (8):

$$\mu = \left|\frac{\varepsilon_y}{\varepsilon_x}\right| = \frac{W_y'/W_y}{W_x'/W_x} \tag{8}$$

where, ε_x is the axial positive strain of the peanut pod samples; ε_y is the transverse positive strain of the peanut pod samples; W_x' is the axial deformation, mm; W_y' is the transverse deformation, mm; W_y is the transverse width of the peanut pods, mm; W_x is the axial length of the peanut pods, mm.

2.5.3 The process of determining the modulus of elasticity and shear modulus

The modulus of elasticity is the proportional relationship between stress and strain during a material's elastic deformation phase. Due to the irregular shape of the peanut pods, a conventional compression test is not possible to measure their cross-sectional area when in contact with the test device. Therefore, the conventional compression test method cannot determine the modulus of elasticity. The apparent modulus of elasticity of peanut pods can be determined using the Hertzian contact stress method according to ASAE S368.4 DEC2000 (R2017) "Compression Test of Food Materials of Convex Shape"[23]. The apparent modulus of elasticity was used to characterize peanut pods' ability to resist deformation produced by external forces. The Hertz equation is generally used with the assumption that the deformation of the material is small. Moreover, the compressed material is elastic.

Ten peanut pods were randomly selected from each of the three types of peanut pods and measured to record their original lengths as X and widths as Y. Peanut pods were compressed using a texturizer (Model TA.XTC-18) produced by Shanghai Baosheng Industrial Development Co. The test was conducted by placing a peanut pod horizontally below the compression probe. The loading speed before contacting the peanut pods was set to 30 mm/min, and it was set to 5 mm/min for contact compression of peanut pods. The trigger force is set to 0.5 N. Compression loading ends when the force-deformation curve exceeds the elastic deformation stage. The return speed after completing compression is set to 50 mm/min. The Hertz equation, as the core of the contact model, has significant advantages in dealing with the normal contact force between particles. The Hertz equation was introduced by Heinrich Hertz in 1882 to describe the normal force-deformation relationship between two elastic spheres in frictionless contact.

The apparent modulus of elasticity of peanut pods can be calculated from the Hertz equation as follows:

$$E=\frac{0.338F\left(1-\mu^2\right)}{D^{3/2}}\left[K_U\left(\frac{1}{R_U}+\frac{1}{R'_U}\right)^{1/3}+K_L\left(\frac{1}{R_L}+\frac{1}{R'_L}\right)^{1/3}\right]^{3/2} \tag{9}$$

where, E is the apparent modulus of elasticity of peanut pods, Pa; F is the compression force applied to peanut pods, N; μ is the Poisson's ratio of peanut pods, which was measured to be 0.386 according to Section 2.5.2; D is the deformation of peanut pods, mm; K_U, K_L are constants, which were obtained from Table 2; R_U, R'_U is the maximum and minimum radius of curvature of the contact point between the convex surface of peanut pods and the upper plate, mm; R_L, R'_L is the maximum and minimum radius of curvature of the contact point between the convex surface of peanut pods and the lower plate, mm.

Table 2 Value of K for various values of θ (adapted from Kozma and Cunningham, 1962)

θ	50	55	60	65	70	75	80	85
K	1.198	1.235	1.267	1.293	1.314	1.331	1.342	1.349

The relationship between cos θ and the radius of curvature of the peanut pod contact is given by the following equation:

$$\cos\theta=\frac{\left[\frac{1}{R_U}-\frac{1}{R'_U}\right]}{\left[\frac{1}{R_U}+\frac{1}{R'_U}+\frac{1}{R_L}+\frac{1}{R'_L}\right]} \tag{10}$$

where, θ is the angle of the main plane at the point of contact between the convex surface of the peanut pod and the flat plate, (°).

Since the shape of the upper and lower surfaces of the peanut pods is essentially the same, the radii of curvature at the point of contact between the convex surface and the flat plate can be considered to be the same. Therefore, Equation (9) can be simplified as follows:

$$E=\frac{0.338F\left(1-\mu^2\right)}{D^{3/2}}\left[2K_U\left(\frac{1}{R_U}+\frac{1}{R'_U}\right)^{1/3}\right]^{3/2} \tag{11}$$

Then the shear modulus G of the peanut pods is:

$$G=\frac{E}{2(1+\mu)} \tag{12}$$

2.6 Physical test determination of exposure parameters

2.6.1 Collision recovery coefficient determination

The collision recovery factor is the post-collision normal partial velocity ratio to the pre-collision normal approach velocity. The collision recovery coefficient is an important parameter for the physico-mechanical characterization of peanut pods[24]. This study used a homemade test setup to carry out experimental measurements based on the theory of collision mechanics of a mass against a stationary surface. The test setup is shown in Figure 4a.

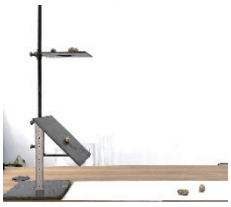

a. Device for determining the coefficient of recovery of peanut pods-65Mn steel plate collision

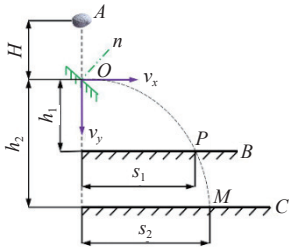

b. Measurement schematic

c. Device for determining the coefficient of recovery of peanut pod-pod collisions

Figure 4 Diagram of experimental setup for the determination of coefficient of recovery of peanut pods collision and principle of determination

The 65Mn steel plate was adjusted to a certain height during the test (the plate was at an angle of 45° to the horizontal). The peanut pods were placed on the release platform with holes. The peanut pods then fall from the holes in a free-fall motion until they collide with 65Mn steel plates. Upon rebounding, the pods will fall to the white paper below. The falling height h_1 and horizontal displacement s_1 of the peanut pods were recorded. The height of the

65Mn steel plate was adjusted to repeat the above test procedure. The falling height h_2 and horizontal displacement s_2 of the peanut pods were then recorded. A high-definition high-speed camera (model: 5F04; resolution: 2320×1720; full-frame acquisition speed: 500 FPS) was used to record the peanut pods' time t from collision point O to drop point P (M). The measurement schematic is shown in Figure 4b.

The device can measure the peanut pod-pod collision recovery coefficient, as shown in Figure 4c. The test principle consistently determines the recovery coefficient for peanut pod-65Mn steel collisions.

2.6.2 Coefficient of static friction determination

The coefficient of static friction is the coefficient of proportionality between the maximum static friction and the positive pressure on the contact surface. In this study, the coefficient of static friction of peanut pods was measured using a homemade test setup using the slant method[25]. The test setup is shown in Figure 5a. The angle is changed by using a wrench to turn the mounting plate mounting screws.

a. Test device for determining the coefficient of static friction

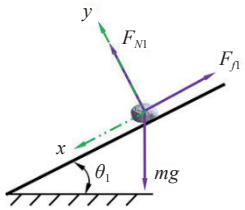

b. Schematic diagram of static friction coef

Figure 5 Test setup for determination of coefficient of static friction of peanut pods and schematic diagram of the determination

The test was conducted by placing peanut pods on 65Mn steel plates. The inclination of the inclined plane is slowly increased by adjusting the steel plate's rotating bolt. As shown in Figure 5b, a protractor reads the inclination angle θ_1 of the incline when the peanut pods tend to slide downward on the incline.

2.6.3 Rolling friction coefficient determination

The coefficient of rolling friction of peanut pods is related to factors such as shape, size, weight, and contact surface characteristics. This study determined the rolling friction coefficient of peanut pods by combining the inclined rolling method with the law of conservation of energy[26]. The test setup is shown in Figure 6a.

The left part of the 65Mn steel plate was tilted at an angle θ_2 during the test. The tilted part of the steel plate was smoothly connected to the horizontal steel plate. The peanut pods were released from the height of the inclined steel plate section H_2. The peanut pods rolled to a stop at the horizontal steel plate S_2. The principle of measurement is shown in Figure 6b. The irregular shape of peanut pods causes them to deviate from the test device after rolling. Therefore, multiple tests are required in this test section. Ten peanut pod rolling datasets which met the requirements were selected for computational analysis.

a. Rolling friction coefficient determination test device

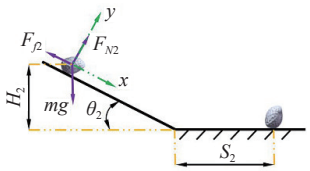

b. Schematic diagram of rolling friction coefficient determination

Figure 6 Test setup for determination of rolling friction coefficient of peanut pods and schematic diagram of the determination

2.7 Stacking angle simulation modeling

When simulation tests are performed using EDEM software, the parameters must be set up first. The time step is taken to be 20%, and the grid size is taken to be 3R. Secondly, a pellet plant needs to be set up. According to the measured proportions of the three types of pods, 900 peanut pod pellets were generated. All particles are generated within 3 s and fall at 0.2 m/s. Cylinder lifting speed is added after peanut pod accumulation has stabilized. At the moment of 3.5 s, the cylinder is lifted at a speed of 0.05 m/s with a uniform velocity. Peanut pods collapse under gravity to form a pod pile. The simulation model of the formed pile angle is shown in Figure 7.

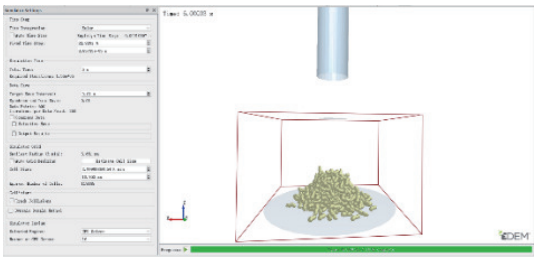

Figure 7 Stacking angle simulation model

3 Results and discussion

3.1 Results of basic physical parameters of peanut pods

3.1.1 Results of the density measurements

The density of each peanut pod was calculated and recorded separately by the measurement method in Section 2.6.1. To minimize measurement error, the final density of peanut pods was taken as the average of all measurements and calculation results. After actual measurements, the density of peanut pods with 36.72% water content at harvest time in saline soil was calculated to be 582.36 kg/m^3.

3.1.2 Results of the Poisson's ratio

Ten randomly selected peanuts from each of the three types of peanut pods were tested for compression. According to Equation (8), the average value was calculated as the final result of Poisson's ratio. The Poisson's ratio of the peanut pods was calculated to be 0.386.

3.1.3 Results of the determination of the modulus of elasticity and shear modulus

The experiment force-compression displacement curve obtained at the end of the compression test is shown in Figure 8.

The selected sample of peanut pods was subjected to repeated tests. The final mean value was taken as the apparent modulus of

elasticity of peanut pods, which was 8.43 MPa after experimental analysis.

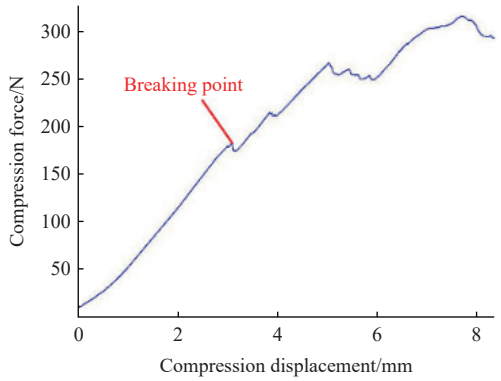

Figure 8 Peanut pods compression test force-displacement curves

Substituting the measured values of modulus of elasticity and Poisson's ratio of the peanut pods into Equation (12), the shear modulus of the peanut pods was found to be 3.04 MPa.

3.2 Results of calibration of contact parameters

3.2.1 Results of collision recovery coefficient measurements

Figure 4b shows that the peanut pods are in free-fall motion between two steel plates with a height difference of H until they come into collision contact with the plates. Neglecting the effect of air resistance, this is obtained from the equations of kinematics:

$$\begin{cases} H = \frac{1}{2}gt^2 \\ v_0 = gt \end{cases} \tag{13}$$

where, H is the falling height of the peanut pods, m; v_0 is the instantaneous speed of the peanut pods before collision, m/s; t is the falling time of the peanut pods, s; g is the acceleration of gravity, m/s^2.

The instantaneous velocity of the peanut pod at the collision point O is:

$$v_0 = \sqrt{2gh} \tag{14}$$

Calculate the horizontal partial velocity v_x and vertical partial velocity v_y of the peanut pods at this point as:

$$\begin{cases} v_x = \sqrt{\frac{gs_1s_2(s_1 - s_2)}{2(h_1s_2 - h_2s_1)}} \\ v_y = \frac{h_1v_x}{s_1} - \frac{gs_1}{2v_x} \end{cases} \tag{15}$$

The peanut pods move in a parabolic motion when they collide with the steel plate:

$$\begin{cases} s_1 = v_xt \\ s_2 = v_yt \\ h_1 = v_xt + \frac{1}{2}gt^2 \\ h_2 = v_yt + \frac{1}{2}gt^2 \end{cases} \tag{16}$$

This is based on the collision recovery coefficient formula:

$$e = \frac{v_n}{v_{n0}} \tag{17}$$

Then the collision recovery coefficient can be found to be:

$$e = \frac{\sqrt{v_x^2 + v_y^2} \cdot \cos\left(45^0 + \arctan\frac{v_y}{v_x}\right)}{v_0 \sin 45^0} \tag{18}$$

According to Equation (18), the collision recovery coefficients between the peanut pods and the 65Mn steel plates ranged from 0.282 to 0.396. The collision recovery coefficients between peanut pods and pods ranged from 0.314 to 0.366.

3.2.2 Results of static friction coefficient measurements

From the force analysis in Figure 5b, the force equilibrium equation of the peanut pod is:

$$\begin{cases} F_{f1} = \varphi F_{N1} \\ F_{N1} = mg\sin\theta_1 \\ F_{N1} = mg\cos\theta_1 \end{cases} \tag{19}$$

where, F_{f1} is the maximum static friction between the peanut pods and the 65Mn steel plate, N; F_{N1} is the maximum support force of the 65Mn steel plate on the peanut pods, N; φ is the coefficient of static friction; m is the mass of the peanut pods, kg; g is the acceleration of gravity, taken as 9.8N/s^2.

According to Equation (19), repeated measurements and calculations yielded static friction coefficients between the peanut pods and the 65Mn steel plates from 0.578 to 0.601. A layer of peanut pods was placed on the surface of a 65Mn steel plate. The principles and measurement steps are the same as those used in the above research process. Thus, the coefficient of static friction between peanut pods and pods can be obtained in the range of 0.837 to 0.878.

3.2.3 Results of rolling friction coefficient measurements

The peanut pods satisfy the law of conservation of energy during rolling, as shown by the force analysis in Figure 6b:

$$mgH_2 = \gamma mg(H_2\cos\theta_2 + S_2) \tag{20}$$

where, H_2 is the height at the release of peanut pods, mm; γ is the coefficient of rolling friction of peanut pods; θ_2 is the inclination angle of 65Mn steel plate, °; S_2 is the rolling distance of peanut pods on the horizontal steel plate, mm.

The rolling friction coefficients of peanut pods and 65Mn steel plates were calculated according to Equation (20) to be in the range of 0.145 to 0.172. A layer of peanut pods was placed on the surface of a 65Mn steel plate. The principles and measurement steps are the same as those used in the above research process. Thus, the coefficient of rolling friction between peanut pods and pods can be obtained from 0.314 to 0.356.

3.3 Screening results and analysis of factors affecting stacking angle

It is important to ensure consistency between the simulation stacking test and the real test results. Therefore, the peanut pods' stacking angle was used as the evaluation index to calibrate the model parameter. The discrete meta-simulation process needs to set more unknown parameters. The Plackett-Burman experimental design can be carried out using Design-Expert software before the test to screen out the factors that significantly influence the simulation process of stacking angle. To reduce the number of Plackett-Burman experimental design parameters in the experiment, the physical parameters were set using the physical parameters related to peanut pods determined in the previous section. The parameters, including Poisson's ratio of peanut pods x_1, shear modulus x_2, coefficient of recovery from collision between pods x_3, coefficient of static friction between pods x_4, coefficient of rolling friction between pods x_5, coefficient of recovery from collision between pods and 65Mn steel plate x_6, coefficient of static friction between pods and 65Mn steel plate x_7, and coefficient of rolling friction between pods and 65Mn steel plate x_8, were used as test factors. Simulated Plackett-Burman tests were carried out using

stacking angle as an evaluation metric. As listed in Table 3, the Plackett-Burman test parameter ranges are listed based on the previous determinations. This experiment had eight influencing factors, so a Plackett-Burman design with a factor number of eleven was selected. Three dummy terms were reserved for error analysis[27]. Table 4 lists the specific test program and results, and Table 5 lists the significance of the test results.

Table 3 Plackett-Burman experiment parameters of peanut pods

Factors	Low	High
Poisson's ratio of peanut pods (x_1)	0.186	0.586
Peanut pods shear modulus (x_2)	1.020	5.060
Peanut pods-pods crash recovery coefficient (x_3)	0.314	0.366
Peanut pods-pods static friction coefficient (x_4)	0.837	0.878
Peanut pods-pods rolling friction coefficient (x_5)	0.314	0.356
Peanut pods-65Mn steel plate crash recovery coefficient (x_6)	0.282	0.396
Peanut pods-65Mn steel plate static friction coefficient (x_7)	0.578	0.601
Peanut pods-65Mn steel plate rolling friction coefficient (x_8)	0.145	0.172
Virtual parameter (x_9)	-	-
Virtual parameter (x_{10})	-	-
Virtual parameter (x_{11})	-	-

Table 4 Scheme and results of Plackett-Burman experiment parameters of peanut pods

Co-de	Factors								Accumulation angle ζ/(°)
	x_1	x_2	x_3	x_4	x_5	x_6	x_7	x_8	
1	0.186	5.06	0.366	0.878	0.314	0.282	0.578	0.172	32.82
2	0.586	5.06	0.366	0.837	0.314	0.282	0.601	0.145	27.16
3	0.186	1.02	0.314	0.878	0.314	0.396	0.601	0.145	35.96
4	0.186	1.02	0.314	0.837	0.314	0.282	0.578	0.145	25.11
5	0.586	5.06	0.314	0.878	0.356	0.396	0.578	0.145	34.78
6	0.186	5.06	0.314	0.878	0.356	0.282	0.601	0.172	36.10
7	0.586	1.02	0.314	0.837	0.356	0.282	0.601	0.172	29.88
8	0.186	5.06	0.366	0.837	0.356	0.396	0.601	0.145	34.39
9	0.586	1.02	0.366	0.878	0.356	0.282	0.578	0.145	39.96
10	0.186	1.02	0.366	0.837	0.356	0.396	0.578	0.172	29.96
11	0.586	1.02	0.366	0.878	0.314	0.396	0.601	0.172	35.51
12	0.586	5.06	0.314	0.837	0.314	0.396	0.578	0.172	22.84

Table 5 Significance analysis of Plackett-Burman characteristic parameters of peanut pods

Source	Sum of squares	df	Mean square	*F*-value	*P*-value	Significance
Model	280.41	8	35.05	19.79	0.0161	*
x_1	1.48	1	1.48	0.83	0.4285	
x_2	5.73	1	5.73	3.23	0.1700	
x_3	19.08	1	19.08	10.77	0.0464	*
x_4	174.73	1	174.73	98.66	0.0022	**
x_5	54.91	1	54.91	31.01	0.0114	*
x_6	0.48	1	0.48	0.27	0.6373	
x_7	15.26	1	15.26	8.61	0.0608	
x_8	8.76	1	8.76	4.94	0.1127	
Residual	5.31	3	1.77			
Cor total	285.73	11				

Note: ** is highly significant (p<0.01); * is significant (0.01≤p<0.05).

As shown in Table 5, the overall model impact is significant. Design-Expert software calculates and analyzes this, showing that the coefficient of determination R^2 is 0.9814. The result of determination R^2 indicates that the test model can be applied to 98.14% of the test data. The significance in Table 5 shows that the effect of x_4 on the simulated stacking angle of peanut pods was extremely significant. Factors x_3 and x_5 significantly affected the simulated stacking angle of peanut pods, while the other factor parameters had less influence. Therefore, factors x_3, x_4, and x_5 were selected for the steepest ascent experiment for further optimization calibration. In carrying out the steepest ascent experiment, the parameters that were not selected for optimization were taken to be the values closest to the true stacking angle test group in the Plackett-Burman test.

3.4 Steepest ascent trial results and analysis

The significant factor parameters selected for optimization were increased stepwise according to the Design-Expert experimental design scheme[28-31]. Three significance parameters were used as test factors. The steepest ascent test was carried out using peanut pod stacking angle, simulation test stacking angle, and bench test stacking angle relative error as evaluation indices. The values of the parameters not selected for optimization are as follows: x_1 is 0.386, x_2 is 3.04 MPa, x_6 is 0.339, x_7 is 0.589, and x_8 is 0.159. Significant influences were selected to take values according to the requirements of the steepest ascent experiment. Equation (21) shows the process of calculating the relative error ψ between the simulation test stacking angle and the bench test stacking angle. The experimental design scheme and results are listed in Table 6.

$$\psi = \frac{|\zeta' - \zeta|}{\zeta} \times 100\% \tag{21}$$

where, ψ is the relative error between the simulation test stacking angle and the bench test stacking angle, %; ζ' is the simulation test value of stacking angle, (°); and ζ is the bench test value of stacking angle, (°).

Table 6 Design and results of steepest ascent experiment

Code	Factors			Accumulation angle ζ/(°)	Relative error ψ/%
	x_3	x_4	x_5		
1	0.314	0.837	0.314	23.89	23.08
2	0.327	0.848	0.332	29.36	5.47
3	0.340	0.858	0.350	31.48	1.35
4	0.353	0.868	0.353	35.01	12.72
5	0.366	0.878	0.356	38.22	23.05

Table 6 shows that the relative error of the stacking angle tends to decrease and then increase with the increasing values of factors. The third set of tests minimized the relative error in stacking angle. In the range of values taken in this group of tests, the simulated stacking angle is slightly larger than the value obtained from the bench test. The stacking angle values obtained by the simulation during the second set of tests were smaller than the true values of the bench tests. Therefore, in conducting the Box-Behnken test, the second set of test levels was taken as the low-level value of the test factor, and the third set of test levels was taken as the high-level value of the test factor.

3.5 Box-Behnken test results and analysis

The analysis of the steepest ascent test results shows that the test parameters were set, as listed in Table 7, while performing the Box-Behnken test. Other parameter settings were the same as those for the steepest ascent test analysis.

Box-Behnken experimental design was performed using Design-Expert software. The experimental program and results are listed in Table 8.

Regression model ANOVA analyzed the Box-Behnken test through Design-Expert software. The results are listed in Table 9.

Table 7 Parameter coding of the Box-Behnken experiment for peanut pods

Level	Factors		
	x_3	x_4	x_5
–1	0.327	0.848	0.332
0	0.334	0.853	0.341
1	0.340	0.858	0.350

Table 8 Scheme and results of Box-Behnken

Code	Factors			Accumulation angle ζ/(°)	Relative error ψ/%
	x_3	x_4	x_5		
1	0.327	0.848	0.341	31.35	0.93
2	0.334	0.853	0.341	30.42	2.06
3	0.334	0.853	0.341	30.02	3.35
4	0.334	0.853	0.341	30.35	2.29
5	0.334	0.848	0.332	29.52	4.96
6	0.327	0.853	0.350	31.84	2.51
7	0.334	0.858	0.332	29.16	6.12
8	0.334	0.853	0.341	30.61	1.45
9	0.327	0.858	0.341	29.93	3.64
10	0.334	0.858	0.350	30.68	1.22
11	0.340	0.848	0.341	29.52	4.96
12	0.334	0.853	0.341	30.86	0.64
13	0.340	0.858	0.341	28.95	6.79
14	0.340	0.853	0.332	28.39	8.60
15	0.340	0.853	0.350	31.26	0.64
16	0.334	0.848	0.350	31.36	0.97
17	0.327	0.853	0.332	29.28	5.73

Table 9 Variance analysis of Box-Behnken experiment regression model

Source	Sum of squares	df	Mean square	*F*-value	*P*-value	Significance
Model	13.92	9	1.55	8.58	0.0049	**
x_3	2.29	1	2.29	12.70	0.0092	**
x_4	1.15	1	1.15	6.36	0.0397	*
x_5	9.66	1	9.66	53.56	0.0002	**
x_3x_4	0.18	1	0.18	1.00	0.3503	
x_3x_5	0.024	1	0.024	0.13	0.7259	
x_4x_5	0.026	1	0.026	0.14	0.7175	
x_3^2	0.27	1	0.27	1.47	0.2645	
x_4^2	0.29	1	0.29	1.62	0.2436	
x_5^2	3.04×10^{-4}	1	3.04×10^{-4}	1.69×10^{-3}	0.9684	
Residual	1.26	7	0.18			
Lack of fit	0.87	3	0.29	2.99	0.1589	
Pure error	0.39	4	0.097			
Cor total	15.18	16				

Note: ** is highly significant (p<0.01); * is significant (0.01≤p<0.05).

Table 9 shows that x_3 and x_5 factors had a highly significant effect on peanut pod stacking angle. The effect of the x_4 factor on stacking angle was significant. The effect of the x_3x_4, x_3x_5, x_4x_5, x_3^2, x_4^2, and x_5^2 factors did not have a significant effect on stacking angle. The p-value for this regression model is 0.0049, which is highly significant. The p-value of the misfit term is 0.1589, which is insignificant. It can be seen that the model has a good fit and no misfit. The regression fitting of the experiment showed that the peanut pod stacking angle had a quadratic regression relationship with the three factors. The second-order regression equation is:

$$\zeta = 30.45 - 0.53x_3 - 0.38x_4 + 1.10x_5 + 0.21x_3x_4 + 0.078x_3x_5 - 0.08x_4x_5 - 0.25x_3^2 - 0.26x_4^2 - 0.009x_5^2 \quad (22)$$

Calculated and analyzed by Design-Expert software, the coefficient of determination R^2 is 0.9169, and the coefficient of variation is 1.41%. The results show that the model accurately reflects the real situation of the test and can be used to carry out stacking angle simulation tests.

3.6 Experimental validation

3.6.1 Peanut pods stacking angle determination

The size of the stacking angle reflects the interaction force between the material particles. The stacking angle is used as an evaluation criterion in the parameter calibration to visualize the basic characteristics of the materials[32]. In this study, the cylinder lifting method was used to obtain the stacking angle of peanut pods. The test was conducted by placing the cylinder vertically on a 65Mn steel plate. Peanut pods were loaded into the cylinder until it was full. The cylinder was lifted at a speed of 0.05 m/s at a constant speed. A camera was utilized to photograph the formation of a peanut pod pile after the cylinder was lifted at a horizontal angle. The captured images are grayed out and binarized, and contour edge coordinates are extracted using Matlab. The slope of the straight line at the edge of the contour obtained after the fitting process is the tangent of the peanut pods' stacking angle[33].

The stacking angle extraction process is shown in Figure 9. The experiment was repeated 10 times. The mean stacking angle ζ of peanut pods was 31.06°.

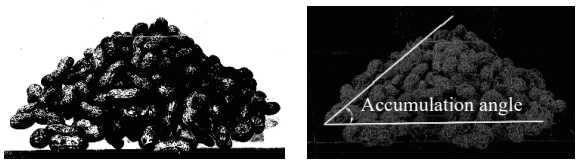

a. Binarized images b. Contour edge extraction

Figure 9 Physical test for determination of peanut pod stacking angle

3.6.2 Comparison of simulation and bench test validation

Optimizing the peanut pod stacking angle through the Optimization Numerical module of Design-Expert software obtained one hundred sets of solutions. The optimized solution is verified by simulating it and comparing the simulated stacking angle values with the bench test values to find the most similar solution. The simulated value of the stacking angle at this point is 30.93°. The error value from the average value of the true stacking angle of 31.06° measured in the bench test is 0.42%. The optimal parameter combinations of the factors in this optimal solution case are: the peanut pods-pods collision recovery coefficient is 0.335, the peanut pods-pods static friction coefficient is 0.854, and the peanut pods-pods rolling friction coefficient is 0.346. Figure 10 shows the peanut pod stacking angle determined in the bench test and the stacking angle determined in the simulation test.

a. Bench test results b. Simulation test results

Figure 10 Plot of peanut pod simulation versus test stacking angle

A comparison of Figures 10a and 10b shows that the angle and shape of the peanut pod stack are basically the same. The results

show that the simulation parameters are set accurately. The calibrated parameters can be used as a reference for studying the material properties of peanut pods using the discrete element method.

4 Conclusions

1) In this study, physical tests were used to determine the basic parameters of salinity-tolerant high-oleic peanut pods of Yuhua 18. The peanut compression test, using a texture meter, obtained the pods' modulus of elasticity and shear modulus. A homemade bench device carried out the collision test and inclined sliding test. We obtained the range of collision recovery coefficient and friction coefficient parameters for peanut pods-65Mn steel, and the range of collision recovery coefficient and friction coefficient for peanut pods-pods were obtained.

2) A simulation test was carried out to calibrate the discrete elemental parameters of peanut pods. The significance parameters affecting pod stacking angle were screened using the Plackett-Burman test, the steepest ascent test, and the Box-Behnken test. A second-order regression model was developed. The optimal parameter combinations of factors affecting the peanut pod stacking angle were obtained using the Optimization Numerical module of Design-Expert software. Optimal simulation model parameters are as follows: the Poisson's ratio of peanut pods is 0.386, the shear modulus is 3.04 MPa, the coefficient of recovery of collision between peanut pods and pods is 0.335, the coefficient of static friction between peanut pods and pods is 0.854, the coefficient of rolling friction between peanut pods and pods is 0.346, the coefficient of recovery of collision between peanut pods and 65Mn steel is 0.339, the coefficient of static friction between peanut pods and 65Mn steel is 0.589, and the coefficient of rolling friction between peanut pods and 65Mn steel is 0.159.

3) The optimal simulation model parameters were utilized for comparative analysis between the validation and bench tests. The results showed that the relative error between the peanut pod stacking angle bench test value and the simulation test value was 0.42%. The results indicate the calibrated peanut pod discrete meta-simulation contact parameters are accurate and credible. They can provide data support for the material characterization of peanut pod discrete elements.

Acknowledgements

We acknowledge that this work was financially sponsored by the National Key Research and Development Program of China (Grant No. 2022YFD2300100), Shandong Province Agricultural Major Technology Collaborative Extension Program Project (Grant No. SDNYXTTG-2024-15), and the National Saline and Alkaline Land Comprehensive Utilization Technology Innovation Center Core Research Team Project (Grant No. NSALCUIC-2024).

[References]

[1] Wang D W, Shang S Q, Zhao D J, Zhu H J. Type-4HBL-4 two-ridges and four-lines semi-feeding self-propelled peanut combine harvester. Transactions of the CSAM, 2013; 44(10): 86–92.

[2] Lu Y G, Wu N, Wang B, Yu Z Y, Lin D Z, Hu Z C. Measurement and analysis of peanuts' restitution coefficient in point-to-plate collision mode. Journal of China Agricultural University, 2016; 21(8): 111–118. (in Chinese)

[3] NBS. 2023 China statistical yearbook; China Statistics Press: Beijing, China, 2023; pp.147–152. (in Chinese)

[4] Zhang H J, Han X, Yang H W, Chen X B, Zhao G Z, Sun J W, et al. Calibrating and simulating contact parameters of the discrete element for apple particles. Transactions of the CSAE, 2024; 40(12): 66–76.

[5] Chang Z C, Sun B, Li D J, Zheng X S, Yan H P, Wang D W, et al. Design and testing of an extruded shaking vibration type pea-nut digging and harvesting machine for saline soil. AgriEngineering, 2024(4): 4182–4202.

[6] Yu J Q, Fu H, Li H, Shen Y F. Application of discrete element method to research and design of working parts of agricultural machines. Transactions of the CSAE, 2005; 21(5): 1–6. (in Chinese)

[7] Zeng Z W, Ma X, Cao X L, Li Z H, Wang X C. Critical review of applications of discrete element method in agricultural engineering. Transactions of the CSAM, 2021; 52(4): 1–20.

[8] Hao J J, Wei W B, Huang P C, Qin J H, Zhao J G. Calibration and experimental verification of discrete element parameters of oil sunflower seeds. Transactions of the CSAE, 2021; 37(12): 36–44.

[9] Horabik J, Molenda M. Parameters and contact models for DEM simulations of agricultural granular materials: A review. Biosyst. Eng, 2016; 147: 206–225.

[10] Li X L, Ji S Y, Duan Q L. International research progress on discrete element methods. Intern. Aca. Develop, 2017(4): 21–23. (in Chinese)

[11] Sun J B, Liu Q, Yang F Z, Liu Z J, Wang Z. Calibration of discrete element simulation parameters of sloping soil on loess plateau and its interaction with rotary tillage components. Transactions of the CSAM, 2022; 53(1): 63–73.

[12] Song Z H, Li H, Yan Y F, Tian F Y, Li Y D, Li F D. Calibration method of contact characteristic parameters of soil in mulberry field based on unequal-diameter particles DEM theory. Transactions of the CSAM, 2022; 53(6): 21–33.

[13] Horabik J, Beczek M, Mazur R, Parafiniuk P, Ryzak M, Molenda M. Determination of the restitution coefficient of seeds and coefficients of viscoelastic Hertz contact models for DEM simulations. Biosyst. Eng, 2017; 161: 106–119.

[14] Zhang G Z, Chen L M, Liu H P, Dong Z, Zhang Q H, Zhou Y. Calibration and experiments of the discrete element simulation parameters for water chestnut. Transactions of the CSAE, 2022; 38(11): 41–50.

[15] Zhang W X, Wang F Y. Parameter calibration of American ginseng seeds for discrete element simulation. Int J Agric & Biol Eng, 2022; 15(6): 16–22.

[16] Jia H L, Deng J Y, Deng Y L, Chen T Y, Wang G, Sun Z J, Guo H. Contact parameter analysis and calibration in discrete element simulation of rice straw. Int J Agric & Biol Eng, 2021; 14(4): 72–81.

[17] Xu F L, He J L, Wang Y H, Li J J, Liu S H, Wu N. Simulation parameters calibration about capsule discrete element model of blue flax. Journal of Gansu Agricultural University, 2021; 56(4): 144–153. (in Chinese)

[18] Zhao S H, Liu H P, Yang C, Yang L L, Gao L L, Yang Y Q. Design and discrete element simulation of interactive layered subsoiler with maize straw returned to filed. Transactions of the CSAM, 2021; 52(3): 75–87.

[19] Guan C S, Fu J J, Xu L, Jiang X Z, Wang S L, Cui Z C. Study on the reduction of soil adhesion and tillage force of bionic cutter teeth in secondary soil crushing. Biosyst. Eng, 2022; 213: 133–147.

[20] Zhu H B, Qian C, Bai L Z, Zhao H R, Ma S J, Zhang X, et al. Design and experiments of active anti-blocking device with forward-reverse rotation. Transactions of the CSAE, 2022; 38(1): 1–11.

[21] Wang G Q, Hao W J, Wang J X. Discrete unit method and its practice on EDEM; Northwestern Polytechnical University Press Co., Ltd: Xi'an, China, 2010. (in Chinese)

[22] Li J W, Tong J, Hu B, Wang H B, Mao C Y, Ma Y H. Calibration of parameters of interaction between clayey black soil with different moisture content and soil-engaging component in northeast China. Transactions of the CSAE, 2019; 35(06): 130–140. (in Chinese)

[23] Joseph St. ASAE S368.4 DEC2000 (R2017): Compression test of food materials of convex shape. American Society of Agricultural and Biological Engineers, 2017.

[24] Xing J J, Zhang R, Wu P, Zhang X R, Dong X H, Chen Y, et al. Parameter calibration of discrete element simulation model for latosol particles in hot areas of Hainan Province. Transactions of the CSAE, 2020; 36(5): 158–166. (in Chinese)

[25] Wu M C, Cong J L, Yan Q, Zhu T, Peng X Y, Wang Y S. Calibration and experiments for discrete element simulation parameters of peanut seed particles. Transactions of the CSAE, 2020; 36(23): 30–38.

[26] Zhang K P, Hou C K, Sun B G, Su Z K. Discrete element simulation parameter calibration of pea grains at harvest time. Agricultural Research in the Arid Areas, 2022; 40(6): 286–294. (in Chinese)

[27] Li Y, Hu C. Experiment design and data processing. Chemical Industry

Press Co., Ltd. Beijing, China, 2017. (in Chinese)

[28] Shen H Y, Gu M, Guo K, Ling J, Gu F W, Pan L, et al. Research on the mechanical properties of peanuts during the harvesting period. AgriEngineering. 2024; 6(3): 3070–3083. DOI: 10.3390/AGRIENGINEERING6030176

[29] Ling J, Gu M, Luo W W, Shen H Y, Hu Z C, Gu F W, et al. Simulation analysis and test of a cleaning device for a fresh-peanut-picking combine harvester based on computational fluid dynamics–discrete element method coupling. Agriculture, 2024; 14(9): 1594.

[30] Chen K, Yin X, Ma W P, Jin C Q, Liao Y Y. Contact parameter calibration for discrete element potato minituber seed simulation. Agriculture, 2024; 14(12): 2298.

[31] Zhang J, Jiang X M, Yu Y J. Modeling method of corn kernel based on discrete element method and its experimental study. Agriculture, 2024; 14(12): 2195.

[32] Liu F Y. Discrete element modelling of the wheat particles and short straw in cleaning devices. PhD thesis, Northwest A&F University, Shaanxi, China, 2018. (in Chinese)

[33] Coetzee C J. Calibration of the discrete element method and the effect of particle shape. Powder Technol, 2017; 310: 104–142.